EI SEVIER

Contents lists available at ScienceDirect

European Journal of Pharmaceutical Sciences

journal homepage: www.elsevier.com/locate/ejps



Multifunctional LUV liposomes decorated for BBB and amyloid targeting. A. In vitro proof-of-concept



Konstantina Papadia ^{a,1}, Eleni Markoutsa ^{a,1}, Spyridon Mourtas ^a, Anastassios D. Giannou ^b, Barabara La Ferla ^c, Fransesco Nicotra ^c, Mario Salmona ^d, Pavlos Klepetsanis ^{a,e}, Georgios T. Stathopoulos ^{b,f}, Sophia G. Antimisiaris ^{a,e,*}

- ^a Laboratory of Pharmaceutical Technology, Department of Pharmacy, University of Patras, Rio 26510, Greece
- b Laboratory for Molecular Respiratory Carcinogenesis, Department of Physiology, Faculty of Medicine, University of Patras, Rio 26504, Greece
- ^c Department of Biotechnology and Biosciences, University of Milano–Bicocca, Piazza dellaScienza 2, 20126 Milan, Italy
- ^d Department of Biochemistry and Molecular Pharmacology, Istituto di RicercheFarmacologiche "Mario Negri", Milan, Italy
- ^e Institute of Chemical Engineering Sciences, FORTH/ICE-HT, Rio 26504, Greece
- f Comprehensive Pneumology Center (CPC), Institute for Lung Biology and Disease (iLBD), University Hospital, Ludwig-Maximilians University, Helmholtz Zentrum München (DZL), Munich, Bavaria 81377, Germany

ARTICLE INFO

Article history: Received 2 December 2016 Received in revised form 27 January 2017 Accepted 9 February 2017 Available online 11 February 2017

Keywords: Nanoparticle Brain Curcumin Targeting Liposomes

ABSTRACT

Multifunctional LUV liposomes (mf-LIPs) were developed, having a curcumin-lipid ligand (TREG) with affinity towards amyloid species, together with ligands to target the transferrin and the LDL receptors of the blood-brain-barrier (BBB), on their surface. mf-LIPs were evaluated for their brain targeting, on hCMEC/D3 monolayers, and for their ability to inhibit A β -peptide aggregation. The transport of mf-LIP across hCMEC/D3 monolayers was similar to that of BBB-LIPs, indicating that the presence of TREG on their surface does not reduce their brain targeting potential. Likewise, mf-LIP inhibitory effect on A β aggregation was similar to that of LIPs functionalized only with TREG, proving that the presence of brain targeting ligands does not reduce the functionality of the amyloid-specific ligand. Addition of the curcumin-lipid in some liposome types was found to enhance their integrity and reduce the effect of serum proteins on their interaction with brain endothelial cells. Finally, preliminary in vivo results confirm the in vitro findings. Concluding, the current results reveal the potential of the specific curcumin-lipid derivative as a component of multifunctional LIPs with efficient brain targeting capability, intended to act as a theragnostic system for AD.

© 2017 Elsevier B.V. All rights reserved.

1. Introduction

The blood-brain barrier (BBB) protects neurons and preserves the CNS, but at the same time prevents drug entry in the CNS (Pardridge, 2016), generating a huge challenge for theragnosis of brain-located pathologies, as Alzheimer's disease (AD). Several non-invasive approaches using nano-particulate carriers have been proposed to overcome this challenge, and some have been successful to delivery higher amounts of drugs (compared to free drug) to the brain (Lalani et al., 2012; Wong et al., 2012; Aparicio-Blanco et al., 2016; Buchwald and Bodor, 2016; Fu et al., 2016; Gutkin et al., 2016; Nair et al., 2016; Saraiva et al., 2016; Tam et al., 2016; Zhang et al., 2016). Recently, liposomes (LIPs) with one ligand to target the transferrin receptor and another to target the low-density-apolipoprotein receptor (LDLr), were

demonstrated to have increased BBB targeting capability, compared to LIPs with one ligand (Markoutsa et al., 2014).

The strategy of utilizing nanoparticulate systems decorated with more than one targeting ligands in order to enhance NP delivery to specific targets, has been successfully explored in several studies (Kibria et al., 2011; Kluza et al., 2012; Li et al., 2012; Bae et al., 2012; Gao et al., 2012), and some types of NPs have been evaluated as theranostic carriers for Alzheimer's disease (AD) (Antimisiaris, 2014; Antimisiaris et al., 2014; Ma et al., 2015; Mourtas et al., 2014). The classic neuropathological signs of Alzheimer's disease are amyloid deposits and neurofibrillary tangles, which consist of the protein fragment beta-amyloid (Aβ-peptides) and tau (a protein normally involved in maintaining the internal structure of the nerve cell), respectively. Most of the nanotechnologies designed for diagnosis and/or therapy of AD up-to-date target the amyloid deposits (AB peptide aggregates) (Antimisiaris et al., 2014). Between the latter, liposomes with a lipid derivative of curcumin (TREG) immobilized on their surface were reported to have very high affinity for AB deposits (Mourtas et al., 2011) and demonstrated a strong inhibitory action towards AB peptide aggregation (Taylor et

^{*} Corresponding author at: University of Patras & FORTH/ICE-HT, Patras, Greece. E-mail address: santimis@upatras.gr (S.G. Antimisiaris).

¹ Equally contributing authors.

al., 2011). However, although the potential of such nanoformulations to interact with amyloid species was proven, and interesting results indicating their therapeutic potential were reported (Balducci et al., 2014; Bana et al., 2014), not much is known about their capability to translocate across the BBB (Koffie et al., 2011; Rotman et al., 2015). Particularly, it has not been studied if the co-presence of AD and BBB targeting ligands on the surface of such multifunctional LIPs affects the functionality of each ligand due to potential interactions between them.

In this context, we prepared herein multifunctional LIPs (mf-LIPs) having three ligands on their surface, by combining two LIP-types studied before; one with the curcumin derivative (TREG) (Mourtas et al., 2011), and another with high affinity for the BBB (Markoutsa et al., 2014). Although such triple-ligand-decorated liposomes are structurally too complicated to be proposed as future therapeutic systems, we selected to use them herein in order to investigate potential interactions between ligands in a highly complicated formulation. Finally we evaluated if, and how, the co-presence of all the ligands on the surface of the mf-LIPs affects their ability to: (i) target the brain and, (ii) inhibit Aβ-peptide aggregation. For each function, the mf-LIPs were compared to the corresponding LIP-type with only one function.

2. Materials and Methods

1,2-distearoyl-sn-glycerol-3-phosphatidylcholine (DSPC), 1,2-distearoyl-sn-glycerol-3-phosphoethanolamine-N-[methoxy (polyethyleneglycol)-2000] [PEG-lipid], 1,2-distearoyl-sn-glycero-3-phosphoethanolamine-N-[maleimide(polyethylene 2000] [PEG-MAL] and lissamine rhodamine B phosphatidylethanolamine [RHO] were purchased from Avanti Polar Lipids. Lipophilic tracer 1,1-dioctadecyl-3,3,3,3-tetramethylindotricarbocyanine iodide [DiR], was from Molecular Probes. Fluorescein-isothiocyanate-dextran-4000 [FITC], Calcein, Lucifer yellow-CH dilithium salt [LY], Sephadex G-50 and Sepharose CL-4B, were from Sigma-Aldrich, Mouse anti-rat CD71 IgG2a (clone OX-26) was obtained from Serotec and anti-mouse CD71 IgG2a (clone RI7217) was from Biolegend. Fetal Calf Serum (FCS) was from Invitrogen. Amicon-Ultra 15 tubes (Millipore) were used for sample concentration. Protein concentrations were measured, by Bradford microassay (Biorad). All other chemicals were obtained from Merck.

Fluorescence intensity (FI) of samples (when needed), was measured by a Shimatzu RF-1501 spectrofluoremeter, using EX-540/EM-590 nm for RHO detection, or EX-490 nm/EM-525 nm for FITC or calcein detection; in all cases 5 nm slits were used. A bath sonicator (Branson) and microtip-probe sonicator (Sonics and Materials) were used for liposome preparation. Bio-fluorescence imaging was done on a PerkinElmer IVIS Spectrum.

2.1. Synthesis and Characterization of ApoE Peptides

An automated peptide synthesizer (Applied Biosystems) at 0.1 mM scale was used for the synthesis of human ApoE peptide (141–150), as previously described in detail (Re et al., 2011). The peptides were synthesized to have a tryptophan residue at the C-terminal utilized for fluorescence detection, and a cysteine residue at the N-terminal utilized for immobilization on the surface of PEG-MAL functionalized LIPs. Fractions containing purified peptides were lyophilized and stored at $-20\,^{\circ}\text{C}$, until their use.

2.2. Synthesis and Characterization of TREG-lipid

For the synthesis of TREG-lipid (see Supplementary Data, and Scheme S1) an updated scaled-up procedure was developed after appropriate modifications of the method described before (Markoutsa et al., 2015).

2.3. Selection of Methodology for mf-LIP Preparation

The different types of liposomes used in the current study are presented in Scheme 1. An optimal methodology to formulate mf-LIPs was developed, after testing different techniques/protocols for attachment of the three ligands on the same vesicle. Two main methods, briefly described below, were tested and the best was selected based on: (i) The attachment yields of the ligands; (ii) The LIP production yield (percent of lipid in mf-LIP in respect to the total amount of lipid used), and (iii) The size distribution of the mf-LIPs. For more details see Supplementary Data.

2.3.1. Method 1 (M1)

TREG was attached on the surface of pre-formed LIPs by a click method, as previously described (Mourtas et al., 2011). Since two additional ligands were planned to be added on the LIP surface (TfR-Mab and ApoE), the pre-formed liposomes had appropriate amounts of maleimide groups on their surface (added as PEG-MAL in their lipid membrane). For attachment of the three ligands, two different protocols were followed. In the first (M1.1), the pre-formed LIPs were incubated with both thiolated-TfR-Mab and ApoE, as previously reported (Markoutsa et al., 2014), and after purification from non-attached ligands by gel filtration (Sepharose4B-CL), the click reaction was carried out for TREG attachment (Mab-ApoE-TREG-LIPs).

In the second protocol (M1.2), the click reaction preceded the attachment of the two brain-targeting ligands and after extensive dialysis (to remove the non-reacted curcumin derivative) the sample was incubated with the TfR-Mab and the ApoE-peptide, and finally purified (from non-attached ligands) (TREG-Mab-ApoE-LIPs).

In all cases, pre-formed liposomes consisted of DSPC/Chol/PEG-lipid/PEG-MAL/PEG-N $_3$ (at 2:1:0.16:0.002 or 0.004:0.2 mol fractions) were formulated by the thin-film hydration technique. For this, appropriate amounts of lipids were dissolved in a CHCl $_3$ /CH $_3$ OH (2/1 v/v) mixture, and the organic solvents were evaporated forming a thin lipid film. The lipid-film was hydrated with PBS pH 7.4 (or FITC or calcein), to produce a liposome dispersion. In some cases, DIR or RHO was added in the lipid phase. Liposome size was reduced by probe sonication, until the liposome dispersions became translucent.

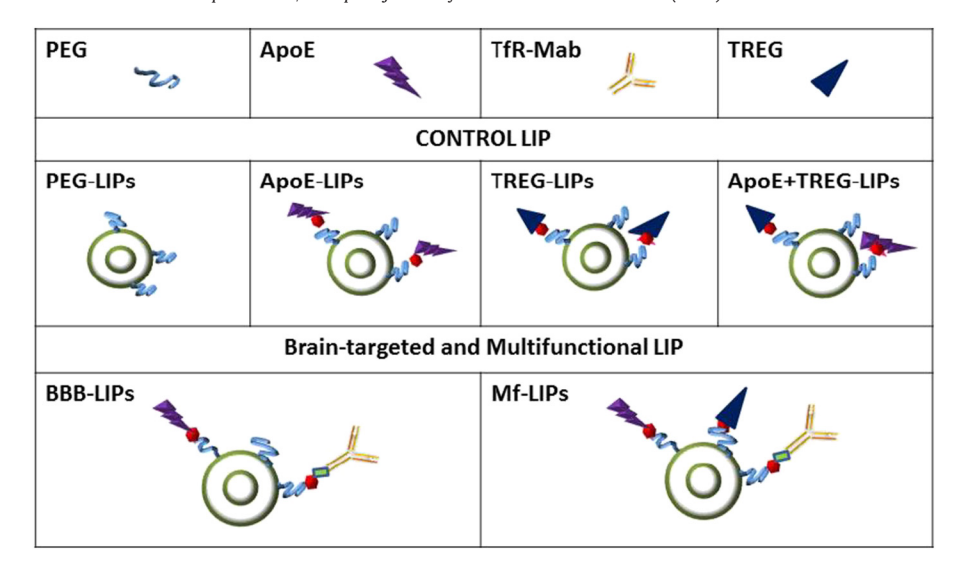
2.3.2. Method 2 (M2)

TREG was initially incorporated in the LIP lipid membrane, after synthesizing a TREG-lipid conjugate (Markoutsa et al., 2015) (see Scheme S1, Supplementary Data). The pre-formed TREG decorated liposomes incorporated the appropriate amounts of PEG-MAL for Mab and ApoE attachment, which was carried out in a second step, as described before (Markoutsa et al., 2014). In more detail, DSPC/Chol/PEG-lipid/PEG-Mal/TREG-lipid (2:1:0.16:0.002-0.004:0.2) TREG-LIPs were prepared, and thiolated-Mab together with ApoE were co-incubated with them overnight at 25 °C. Finally, non-attached fractions of Mab and ApoE were removed from LIPs by ultracentrifugation at 40,000 rpm for 2×30 min.

2.4. Physicochemical Characterization of mf-LIPs

2.4.1. Ligand Attachment and Production Yield

For calculation of ligand attachment: (i) The Mab attachment yield was calculated following purification of LIPs from non-attached Mab, by an Elisa technique, as previously described (Markoutsa et al., 2011, 2012, 2014). (ii) The ApoE attachment yield was measured by the fluorescence intensity ($\lambda_{ex}=280$ nm; $\lambda_{em}=350$ nm) of the peptide, using known amounts of peptides dissolved in buffer for calculation of peptide concentration (Re et al., 2011; Markoutsa et al., 2014). (iii) The quantification of TREG in purified liposomal dispersions was achieved by HPLC (Shimatzu, LC20) performed with a Lichrosphere100 RP-18 5 μm column, eluted with CHCl3/MeOH (9:1) with 0.08% TFA as mobile phase, at 1 ml/min.



Scheme 1. Schematic representation of the various types of Liposomes (LIPs) constructed.

The production yield, which is the percent of mf-LIP lipid compared to the initial total amount of lipid used, was calculated by measuring the exact lipid amount in the initial lipid mixture used for liposome preparation and in the mf-LIP dispersions, by the Stewart assay (Stewart, 1980).

2.4.2. LIP Size Distribution and z-Potential

Particle size distribution was measured by dynamic light scattering (DLS) (Malvern Nano-zeta) at 25 °C and at an angle of 173°, in diluted (0.4 mg/ml) LIP dispersions, using 10 mM PBS, pH 7.40. The ζ -potential of LIPs was measured at 25 °C by the same instrument, utilizing the Doppler electrophoresis technique.

2.4.3. LIP Integrity Studies

LIP integrity was evaluated by measuring the retention of vesicleentrapped calcein or membrane-associated DiR, during incubation in buffer or FCS (80% w/w) for 48 h at 37 °C, at a lipid concentration of 1 mg/ml. Calcein latency and retention was measured at selected time points, as reported before (Kokona et al., 2000). In the case of DiR-loaded vesicles, the retention of DiR was measured (at selected time points) by drawing 100 uL samples from incubation tubes, placing the samples in 96 well plates, and acquiring bio-fluorescence images of the plates on an IVIS Lumina II imager (Perkin Elmer, Santa Clara, CA), using excitation/emission wavelengths to detect DiR (EX: 710-760 nm; EM: 810-875 nm). Images were analyzed by Living Image v4.2 software (Perkin Elmer, Santa Clara, CA) and specific regions of interest (SOPs) for each well plate were created and were superimposed over all images acquired (during different time-points), in a uniform fashion. Subsequently, photon fluxes within these regions were measured and compared between the different time points, after subtraction of photon fluxes measured for empty plates (blank). DiR retention was calculated from each photon flux value, as the percent of the value measured for the same sample at time 0.

2.5. Inhibition of Aβ1-42 Peptide Aggregation by mf-LIPs

The thioflavin-T assay was performed on de-seeded A β 1-42 peptides (Manzoni et al., 2009; Markoutsa et al., 2015). In brief, 2 mg aliquots of recombinant A β 1-42 peptides (kindly provided by Mario-Negri Institute, Milan, IT) were dissolved in 0.5 ml of trifluoroacetic acid/thioanisole 95.5:4.5 (v/v) and kept on ice for 60 min. After that, 167 ml of pure ice-cold formic acid were added, and the mixture was vortexed and kept in an ice bath for another 20 min. Peptides were collected by centrifugation (15 min, 13,000 rpm), and then they were re-

dissolved in $\rm H_2O/acetonitrile~50:50~(v/v)$ and lyophilized. Age reversed peptides were used immediately. The Thioflavin T assay was conducted in clear-bottom 96-well microtiter plates. For this, LIPs (40 mM), A β 1-42 peptides (25 mM), and thioflavin-T (15 mM) were placed in a final volume of 100 μ l of PBS (10 mM, pH 7.4), and aggregation was monitored at 30 °C over a period of 96 h by measuring thioflavin-T fluorescence every 24 h (TECAN InfiniTE-M200 plate reader [EX-450 nm, EM-482 nm]).

2.6. Brain Targeting Potential of mf-LIPs

Immortalized human brain capillary endothelial cells (hCMEC/D3) (passage 25–35) were used as a cellular model of the BBB (Markoutsa et al., 2011, 2012). The cell line was obtained under license from Institut National de la Santé et de la Recherche Médicale (INSERM, Paris, France). Cells were seeded at 200,000 cells per insert (40,000–50,000 cells/cm²); 37 °C in 5% CO $_2$ and grown in EndoGROTH-MV Complete Culture Media Kit® (Millipore #SCME004) supplemented with -bFGF: human Basic Fibroblast Growth Factor (Sigma, #F0291), Penicillin, 10,000 units and Streptomycin, 10,000 µg/ml (Life technologies, #15140–122). The cells were cultured at 37 °C and 5% CO $_2$ saturated humidity. All culture ware were coated with Cultrex® Rat Collagen I lower viscosity (R&D Systems, Trevigen, #3443–100–01) for 1 h, and then washed with PBS and replaced with complete culture medium. Medium was changed every 2–3 days.

2.6.1. Cell Uptake Studies

FITC-dextran-containing vesicles were incubated with confluent monolayers of hCMEC/D3 cells (200 nmoles liposomal lipid/ 10^6 cells) in medium containing 5% (v/v) FCS, at 37 °C for 60 min, then washed in ice-cold PBS (×3), detached from plates, re-suspended in PBS and assayed for FITC-FI (after cell lysis in 2% Triton X-100). Cell auto fluorescence was always subtracted. Control experiments were carried out with free FITC-dextran at similar amounts with those encapsulated in the LIPs, in order to exclude the possibility of uptake of dye that leaks out from LIPs; the FI values measured in the control experiments were null.

In a second set of experiments the uptake of LIPs was evaluated in presence of cell medium that was supplemented with increased amounts of FCS (20% and 50% v/v). All other conditions were kept constant.

2.6.2. Cell-monolayer Permeation Studies

Cell monolayers were developed by seeding hCMEC/D3 cells on type I collagen pre-coated Culture inserts (Corning #3450 6-multiwell PET

plates with 0.4 μ m porosity) at a density of $4-5 \times 10^4$ cells/cm². Medium was changed at day 3, and transport assays were performed 6-7 days after seeding, when the Trans-Endothelial Electrical Resistance (TEER) reached a plateau value; 24 h before each experiment, the cell medium was replaced with fresh medium containing 1 nM simvastatin. Monolayer integrity was periodically inspected with a microscope and the TEER was monitored by a Millicell ERS-2 (Millipore). The monolayer quality was confirmed by measuring LY permeability, as described before (Markoutsa et al., 2011). Transport experiments were conducted in HBSS (PBS + MgCl₂ and CaCl₂) supplemented with 10 mM HEPES and 1 mM sodium pyruvate. Transport was estimated after placing LIPs (labeled with RHO, or with DiR) on the upper side of monolayers (200 nmoles lipid/well) and measuring RHO or DiR-FI. FITC was not used for measurement of LIP-transport, since the size of liposomes was recently demonstrated to influence their transport across hCMEC/ D3 monolayers (Papadia et al., 2016), and size of FITC-entrapping LIPs with TREG-lipid in their membrane were substantially larger compared to the LIPs without TREG, which were used as controls. In all cases LY permeability was calculated simultaneously with LIP transport, to ensure that the vesicles did not disrupt the barrier, enhancing paracellular transport.

2.7. Cytotoxicity Assay

The cytotoxicity of TREG-LIPs and mf-LIPs towards hCMEC/D3 and HEK cells (Human embryonic kidney cells 293) was evaluated by the MTT assay (Markoutsa et al., 2014). For this, HEK cells were cultured in RPMI 1640 medium with 5% (v/v) FCS at 37 °C and 5% CO $_2$ saturated humidity. BBB-LIPs were not studied, since they were previously found to be non-cytotoxic when incubated with hCMEC/D3 under identical conditions (with those applying in the current studies) (Markoutsa et al., 2014).

2.8. Preliminary In Vivo Brain Distribution Study

A preliminary in vivo live animal imaging experiment was carried out, to compare brain distribution of mf-LIPs and BBB-LIPs, both incorporating DiR, in FVB mice. FVB mice, chosen for their white skin and fur that permits enhanced light penetrance, were purchased from Hellenic Pasteur Institute (Athens, Greece) and bred at the Center for Animal Models of Disease, University of Patras, Faculty of Medicine (Rio, Greece). Animal care and experimental procedures were approved by the Veterinary Administration Bureau of the Prefecture of Achaia, Greece, and were conducted according to European Union Directive 86/609/EEC for animal experiments (http://ec.europa.eu/ environment/chemicals/lab_animals/legislation_en.htm). Mice used for experiments were sex-, weight (20-25 g)-, and age (6-8 weeks)-matched, and randomly allocated to treatment with 0.05 mg of each LIP-type/mouse, via tail vein injection (n = 3-5mice/group). Bio-fluorescence imaging of living mice was done on an IVIS Lumina II imager (Perkin Elmer, Santa Clara, CA). At specific time points, mice were anesthetized using isoflurane and serially imaged, using excitation/emission wavelengths to detect DiR (excitation: 710-760 nm; emission: 810-875 nm). Images were acquired and analyzed using Living Image v4.2 software (Perkin Elmer, Santa Clara, CA). In detail, brain specific regions of interest were created and superimposed over all images acquired in a uniform fashion. Subsequently, photon flux within these regions was measured and compared between mice receiving different treatments. Brain DiR signals were normalized to DiR dose. The latter was measured by placing the specific amount injected in a well of a 96-well plate and measuring the biofluorescence signal of the DiR in the same way as measured in the animals (identical size of ROIs were used for the different formulations).

2.9. Statistical Analysis

All results are expressed as mean \pm SD from at least three independent experiments. The significance of variability between results from various groups was determined by two-way-ANOVA, and individual differences between groups were tested by Tukey's multiple comparisons test (SPSS Statistics, 2.4, IBM).

3. Results

3.1. Selection of Optimized Methodology for mf-LIPs

As seen in the results presented in Table 1, the attachment of TREG on LIPs by Method 2 (pre-synthesis of the TREG-lipid conjugate), resulted in a dramatic increase in lipid recovery compared to Method 1. Furthermore, the LIPs formulated by Method 2 had mean diameters below 200 nm, and good attachment yields for all three ligands (TREG: $89.3\pm1.2\%$; TfR-Mab: 67.3 ± 8.0 ; ApoE: 86.7 ± 7.8), thus Method 2 was used for preparation of mf-LIPs. The LIP-attachment yields for Mab and ApoE on mf-LIPs (prepared by Method 2) were similar to those reported earlier for the BBB-targeted LIPs (Markoutsa et al., 2014), suggesting that the incorporation of the TREG in the liposome bilayer did not prevent the immobilization of the two additional ligands via MAL-thiol interaction.

3.2. Physicochemical Properties and Integrity of mf-LIPs

The mean diameters of all LIPs used (in in vitro and in vivo experiments) were below 155 nm, as seen in Table 2. mf-LIPs were slightly larger compared to all other LIP types (PEG-LIPs, BBB-LIPs and TREG-LIPs), which is logical due to the presence of three ligands on their surface. BBB-LIPs and mf-LIPs with surface densities of BBB-targeting ligands equal to 0.1 mol% (MONO density) and 0.2 mol% (DOUBLE density), were constructed. As expected, the DOUBLE density LIPs were slightly larger (their mean diameter was increased by 14–29%) compared to the corresponding MONO density LIPs. In all cases, the polydispersity index (PDI) was low (compared to usual values measured in liposome dispersions) (Table 2).

In terms of morphology, BBB-LIPs were previously found to be unilamellar, by Transmission Electron Microscopy observation (Markoutsa et al., 2014), while a similar morphology was observed for mf-LIPs (not shown).

The integrity of mf-LIPs was evaluated during incubation in absence (PBS) and presence of serum proteins (80% of FCS v/v) and compared to that of TREG-LIPs (Fig. 1.A) and BBB-LIPs (Fig. 1.B). As seen in Fig. 1.A the retention of calcein, a small-molecule hydrophilic dye, in both LIP-types is very high when they are incubated in buffer, however there is a gradual release of the dye from the vesicles when they are incubated in presence of serum proteins (fetal calf serum, FCS), especially after 24 h. Furthermore, the integrity of DOUBLE density vesicles is lower compared to that of corresponding MONO density vesicles, for both, mf-LIPs (Fig. 1.A) and BBB-LIPs (Fig. 1.B). The integrity of MONO density mf-LIPs and BBB-LIPs in FCS is similar, suggesting that the presence of TREG-lipid in the lipid-bilayer does not affect the vesicle integrity. In fact 24 h post-incubation, calcein retention is higher in DOUBLE density mf-LIPs (69.6 \pm 5.4%) compared to the corresponding BBB-LIPs (49 \pm 11%), indicating that the inclusion of TREG-lipid in the lipid-membrane may have a stabilizing effect on the vesicles (at least in respect to the leakage of vesicle-entrapped calcein). As seen in Fig. 1.C, a similar behavior is observed for DiR retention in DOUBLE density mf-LIPs and BBB-LIPs.

3.3. Inhibition of Aβ1-42 Aggregation by mf-LIPs

mf-LIPs were demonstrated to inhibit Aβ1-42 peptide aggregation, while the corresponding (control) PEG-LIPs, with no amyloid-specific

Table 1

Attachment yields of Mab, ApoE and TREG, and Lipid recovery (or production yield) of LIPs prepared by the different methods described in the Methods section. The LIP naming denotes the sequence of attachment for the different ligands.

LIP composition	Mean diameter (nm)	PDI	Mab yield (% attached)	ApoE yield (% attached)	TREG yield (% attached)	Lipid recovery (%)		
Method 1 (attaching TREG by click method after (M1.1) or before (M1.2) decoration with ApoE & Mab)								
ApoE-Mab/TREG (M1.1)	1900 ± 122	0.603 ± 0.089	59.4 ± 5.8	87.5 ^b	51	21-24		
TREG/ApoE-Mab (M1.2)	a	a	55.1 ± 4.2^{b}	83.44 ^b	50	a		
Method 2 (attaching TREG [synthesized in organic solution] by incorporation in lipid phase of LIPs during their initial formation)								
(M2)	149 ± 25	0.242 ± 0.038	67.3 ± 8.0	86.7 ± 7.8	89.3 ± 1.2	80-95		

^a Liposome size was too big to measure with DLS and the lipid recovery was <10%.

ligands on their surface, did not acquire any effect on the rate or extent of peptide aggregation (Fig. 2), as reported earlier (Markoutsa et al., 2015). When comparing the extent of peptide aggregation in presence of TREG-LIPs and mf-LIPs it is seen that although the effect of mf-LIPs on peptide aggregation is initiated after 48 h, after 96 h of co-incubation both vesicle types completely inhibit A β -peptide aggregation. This finding indicates that the co-presence of the two BBB-targeting ligands on the surface of mf-LIPs does not reduce the functionality of the curcumin-lipid derivative to inhibit A β -peptide aggregation.

3.4. BBB Targeting Potential of mf-LIPs (In Vitro)

3.4.1. Cytotoxicity of mf-LIPs

PEG-LIPs and BBB-LIPs have been previously reported to be non-cytotoxic. TREG-LIPs and mf-LIPs were tested for their cytotoxicity towards hCMEC/D3 and HEK cells (by the MTT assay) when coincubated with cells for 24 h, at similar concentrations with those used in the LIP/cell interaction studies. Results indicate that both LIP-types are non-cytotoxic, opposed to Triton X-100 (1% w/w) which is used as a positive control (Fig. 3).

3.4.2. Uptake of mf-LIPs by hCMEC/D3 Cells

The uptake of mf-LIPs by hCMEC/D3 cells is slightly lower (~15%) than the uptake of BBB-LIPs, indicating that the co-presence of TREG in the bilayer of BBB-LIPs may cause a slight reduction on their braintargeting capability (Fig. 4.A). Uptake values of BBB-LIPs and PEG-LIPs are similar to those reported before (Markoutsa et al., 2014). Interestingly, the uptake of TREG-LIPs by hCMEC/D3 cells is 1.94 times higher than that of PEG-LIPs, although TREG-LIPs do not have any BBB targeting ligand on their surface. A similar BBB-targeting effect was also observed before in another type of amyloid-targeting LIPs, and was proven to implicate the RAGE transporter which is responsible for the transport of amyloid peptides from the blood to the brain (Markoutsa et al., 2012).

Previously, it was demonstrated that the uptake of different braintargeted-LIPs by hCMEC/D3 cells was affected in a different way, when the uptake experiment was carried out in presence of serum proteins

Table 2Physicochemical properties of mf-LIPs and the various LIPs constructed to be used as controls. As control LIPs, plain LIPs with only PEG and no ligands on their surface (PEG-LIP), LIPs with only TREG-lipid (TREG-LIPs) and LIPs with only the two brain-targeting ligands (BBB-LIPs), were used. BBB-LIPs and mf-LIPs with 0.1 or 0.2 (mole %) concentration of BBB-targeting ligands were constructed and are referred to as MONO or DOUBLE density LIPs, respectively. Size distribution [mean hydrodynamic diameter and polydispersity index (PDI)] and zeta-potential values reported, are mean values from at least 4 different preparations.

LIP Type	Mean hydrodynamic diameter (nm)	PDI	ζ-Potential (mV)
PEG-LIPs	105.6 ± 5.7	0.125 ± 0.019	-2.47 ± 0.523
TREG-LIPs	111.8 ± 2.5	0.270 ± 0.062	-3.27 ± 0.148
BBB-LIPs(mono)	111.9 ± 3.8	0.172 ± 0.045	-3.01 ± 0.72
mf-LIPs _(mono)	136 ± 18	0.131 ± 0.054	-3.71 ± 0.72
BBB-LIPs _(double)	145 ± 13	0.205 ± 0.045	-3.35 ± 0.44
mf-LIPs _(double)	155 ± 30	0.213 ± 0.055	-3.31 ± 1.51

(20%–50% v/v FCS). In order to see how the addition of TREG in the membrane of the various types of brain-targeted-LIPs, affects their uptake by hCMEC/D3 cells under such conditions, we measured the uptake of ApoE-LIPs, ApoE+TREG-LIPs, BBB-LIPs and mf-LIPs in cell culture medium containing 20% and 50% (v/v) FCS. As demonstrated in Fig. 4.B, while the uptake of BBB-LIPs was significantly reduced (P = 0.013) when FCS concentration was increased from 5 to 50%, in agreement with previous results (Markoutsa et al., 2014), the effect of serum proteins on the uptake of mf-LIPs is null. The later result suggests that the addition of TREG in the bilayer of BBB-LIPs modulates their surface and minimizes their interaction with serum proteins (or at least with those proteins that are implicated in reduced uptake of LIPs by targeted cells). In fact, the previous suggestion is additionally supported by the increased integrity (during incubation in presence of FCS) of mf-LIPs, compared to BBB-LIPs, demonstrated by the calcein retention experiments (Fig. 1.C).

In order to test the above theory, the effect of adding TREG on the surface of ApoE-LIPs was studied. ApoE-LIPs were selected, since their uptake by hCMEC/D3 cells was previously found to be highly affected by serum proteins (Markoutsa et al., 2014). ApoE+TREG-LIPs were prepared (by the same method applied for mf-LIP preparation), and interestingly their uptake by hCMEC/D3 cells was not modified by the presence of serum proteins although the uptake of ApoE-LIPs was reduced by 59% as FCS increased from 5% to 50% v/v, in-line with previous findings (Markoutsa et al., 2014), suggesting that the addition of TREG in the bilayer of ApoE-LIPs modulates their surface and minimizes their interaction with serum proteins (Fig. 4.C), as seen for BBB-LIPs.

3.4.3. Transport of mf-LIPs Across hCMEC/D3 Monolayers

The trans-endothelial electrical resistance (TEER) of the monolayer (after simvastatin treatment and before the experiment) was 61.0 \pm 3.9 Ω cm² and 59.8 \pm 3.2 Ω cm² after the experiment, while LY permeability was 1.103 \times 10 $^{-3}$ \pm 1.18 \times 10 $^{-4}$ cm/min; all values in good agreement with previous reports (Poller et al., 2008; Markoutsa et al., 2011, 2014). LY permeability was also measured concurrently with LIP transport, and no significant differences were detected in any case, proving that monolayer permeability was not affected by any of the LIP-types tested.

As seen in Fig. 5 for all LIP types there is a gradual increase in transport of LIP-associated RHO, with time. The permeability values calculated from the transport results were $3.01 \times 10^{-5} \pm 0.59 \times 10^{-5}$ cm/min for PEG-LIPs; $5.78 \times 10^{-5} \pm 0.58 \times 10^{-5}$ cm/min for TREG LIPs; $19.03 \times 10^{-5} \pm 2.8 \times 10^{-5}$ cm/min for BBB-LIPs and $25.1 \times 10^{-5} \pm 3.2 \times 10^{-5}$ cm/min for mf-LIPs. The permeability values of PEG-LIPs and BBB-LIPs are similar with those reported before (Markoutsa et al., 2012, 2014). TREG-LIP permeability, is approx. 2 times higher than PEG-LIP permeability, while mf-LIP permeability is slightly higher than that of BBB-LIPs, but the difference is not statistically significant (P = 0.054). In fact, when the transport values of MONO density and DOUBLE density mf-LIPs are compared with the values of corresponding BBB-LIPs (Fig. 5.B), they overlap in both cases. Thereby, it is concluded that the addition of TREG in the membrane of BBB-LIPs does not affect their potential to translocate across the BBB.

b Attachment yields were calculated as % attached/lipid and thereby in samples where lipid recovery was very low (<10%) the amounts measured were very low, so the values may not be accurate.

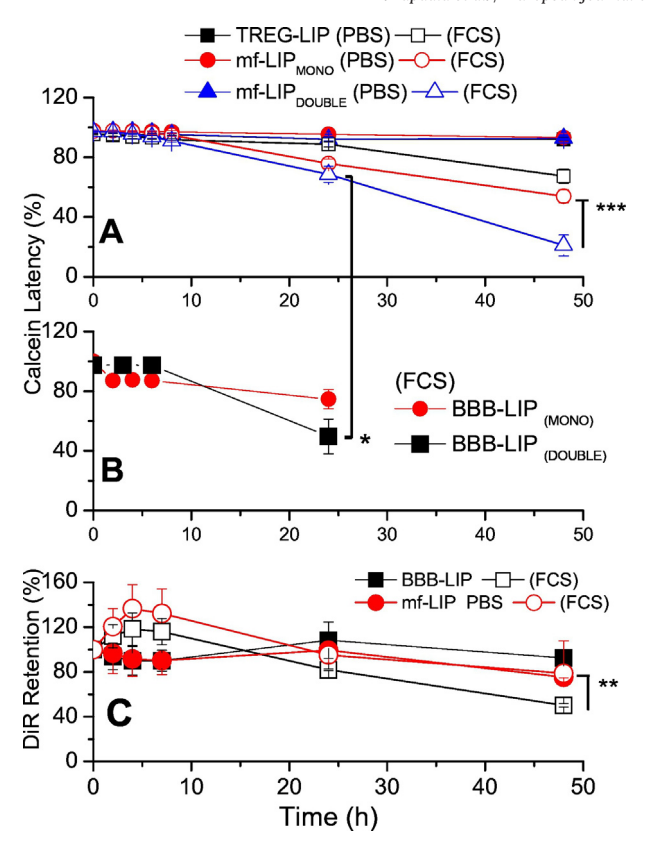


Fig. 1. Retention of dye (calcein or DiR) in various LIP types (see Figure insets for key) during incubation of the LIPs at 37 °C, with buffer (solid symbols) or with 80% v/v Fetal Calf Serum (FCS) (hollow symbols), for periods up to 48 h. Retention of calcein (expressed as calcein latency %) in TREG-LIPs and mf-LIPs is seen in graph A, and in BBB-LIPs, in graph B. Retention of DiR (%) in mf-LIPs and BBB-LIPs is seen in graph C. Each value is the mean of 3 samples, and bars represent SDs of mean. Asterisks denote significant differences between specified samples ($^{\rm FP} \le 0.05$, $^{\rm FP} \le 0.01$, $^{\rm FP} \le 0.01$).

When compared with results from other studies in which the same cellular model of BBB is used, the permeability results obtained herein for BBB-LIPs and mf-LIPs are up to five times higher than those reported for non-targeted and targeted (with anti-PECAN-1 antibody) iron oxide NPs, which were between 2.4×10^{-5} and 4.2×10^{-5} cm/min, when transport was studied over a 6 hour period (Dan et al., 2013). Liposomes having the anti-TfR Mab on their surface were tested on hCMEC/D3

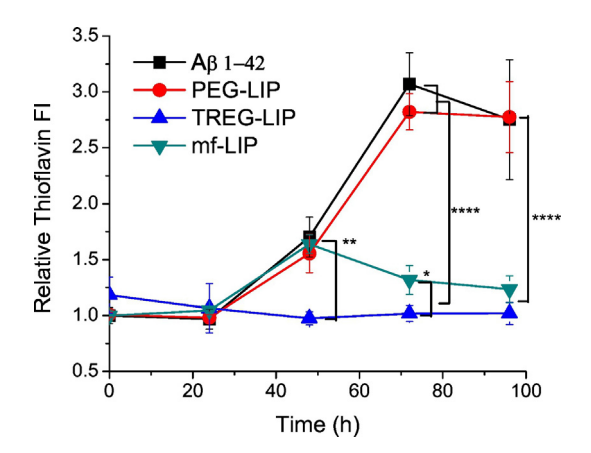


Fig. 2. Aggregation of Aβ1-42 peptides, measured as relative Thioflavin FI (ThT assay) during a 96 h time course in absence and presence of various types of LIPs. Plain PEG-LIPs were used as control vesicles; TREG-LIPs and mf-LIPs were compared for their capability to inhibit Aβ1-42 aggregation. Each value is the mean value calculated from at least 3 different experiments and SD values are presented as bars. Asterisks denote significant differences between specified samples (*P \leq 0.05, **P \leq 0.01, ***P \leq 0.001).

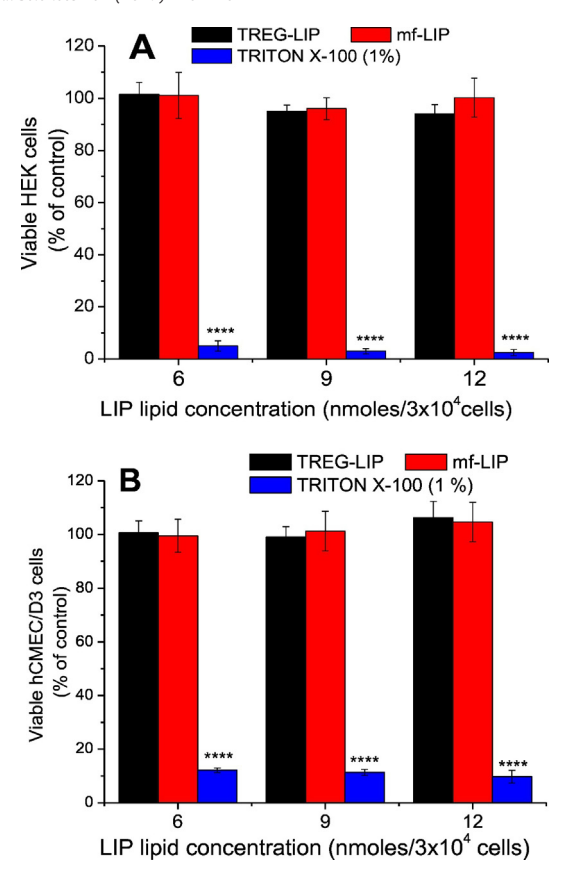


Fig. 3. Cytotoxicity (number of viable cells expressed as percent of the viable cells in the control wells [in which cells are incubated with plain PBS]) of TREG-LIPs and mf-LIPs towards HEK (A) and hCMEC/D3 cells (B), measured by the MTT assay, after 24 h incubation of the LIPs (3–9 nmoles of LIP-lipid/ 3×10^4 cells). Each value is the mean of 4 different samples, and column bars represent the standard deviation of each mean. Asterisks denote significant differences between specified samples (*P \leq 0.05, **P \leq 0.01, ***P \leq 0.001).

monolayers before (Salvati et al., 2013b), and a much lower permeability value, approx. 8×10^{-6} cm/min, was calculated over 2 h of incubation. This value is >20 times lower compared to the permeability of BBB-LIPs obtained herein. In addition to the fact that BBB-LIPs have two brain-specific ligands on their surface, the substantial difference in permeability values between the previous study and our study, is most probably also connected with the fact that the previous liposomes had a different lipid composition, which conferred a highly negative surface charge. In another study, when 50 nm SiO₂ nanoparticles were tested for 4 h, 3.6% of the initial mass reached the basal chamber of the hCMEC/D3 monolayer system, while the value was 1.7% and 1.1% for 100 nm and 200 nm SiO₂ nanoparticles, respectively (Ye et al., 2013). The latter values are similar to the (% transport) values measured in the cases of the non-targeted LIPs used herein, when taking into account their size and the fact that our studies were carried out over a 2 hour period.

3.5. Preliminary In Vivo Study

In Fig. 6 the brain signals for DiR, measured at various time points, post-injection of 0.05 mg/animal of mf-LIPs or BBB-LIPs, are shown, expressed as DiR signals (in Photons/s) (A) or normalized for the injected DiR dose (B). LIP with DOUBLE surface-density of the braintargeting ligands, were used. As seen, despite the slightly higher signals measured after mf-LIP injection (compared to the DiR signal of BBB-LIPs), there are no statistically significant differences in head-DiR signals between mf-LIPs and BBB-LIPs (P = 0.9635), suggesting that the

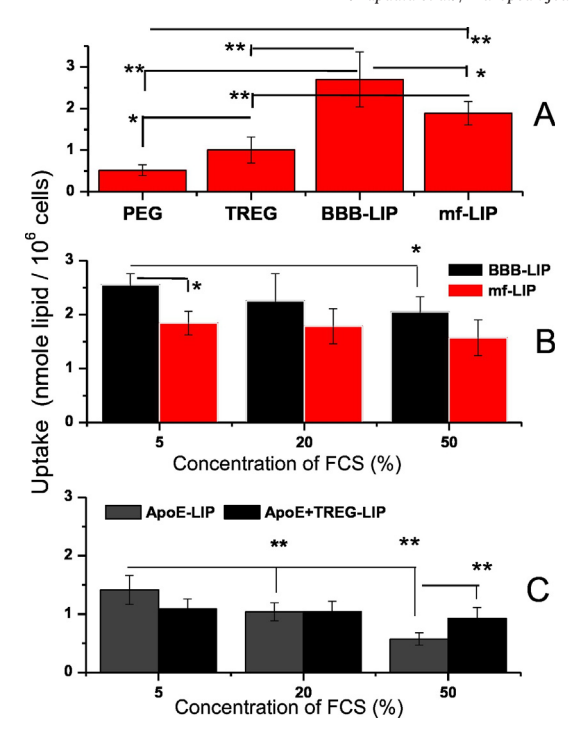


Fig. 4. A] Uptake of mf-LIPs PEG-LIPs and BBB-LIPs (nmoles of liposomal lipid), by hCMEC/D3 cells, after 1 h incubation of 200 nmoles of lipid/1 \times 10⁶ cells (in medium containing 5% FCS). B & C] Uptake of BBB-LIPs and mf-LIPs (B), as well as ApoE-LIPs and ApoE+TREG-LIPs (C) by hCMEC/D3 cells, in presence of increasing amounts of FCS (5%, 20% and 50%). In the case of BBB-LIPs and mf-LIPs the 0.1 mol% density (MONO) of the BBB-specific ligands was used. Each result is the mean of at least 6 different samples and the corresponding SD of the means are added as bars. Asterisks denote significant differences between specified samples (*P \leq 0.05, **P \leq 0.001).

addition of TREG-lipid in the brain-targeted liposomes, does not modulate their brain targeting potential.

4. Discussion

Multifunctional liposomes (mf-LIPs) with both amyloid and BBB affinity, consisting of a curcumin-derivative referred to as TREG (Mourtas et al., 2011; Taylor et al., 2011) and two BBB-targeting ligands (Markoutsa et al., 2014), were prepared in order to evaluate the effect of the co-presence of different ligands on their functionalities. Initially, an optimal methodology was identified for the preparation of sufficiently stable vesicles, which were subsequently evaluated for their capability to: (i) inhibit A β -peptide aggregation and (ii) target the BBB. The BBB-LIPs used herein, were previously demonstrated to have significantly higher capability to target the BBB, compared to PEG-LIPs (in vitro, in vivo and ex-vivo) (Markoutsa et al., 2014).

From the in vitro studies performed, it is concluded that: (i) The copresence of TREG with the BBB targeting ligands (TfR-Mab and ApoE) on the surface of mf-LIPs does not prevent the interaction between TREG and A\beta-peptides (when mf-LIPs are incubated with A\beta-peptides) and complete inhibition of peptide aggregation is achieved (equivalent to that achieved by plain TREG-LIPs) (Fig. 2). This result is particularly important since other mf-liposomes that were decorated with another curcumin-lipid derivative, referred to as DPS-curcumin (Lazar et al., 2013) were found to loss a significant percent of their capability to inhibit Aβ-peptide aggregation when only one BBB-targeting ligand (the same TfR-Mab used in the current study) was added on their surface (Mourtas et al., 2014). (ii) TREG-LIPs demonstrate increased uptake by hCMEC/D3 cells (Fig. 4) and increased transport across cell monolayers (Fig. 5) compared to control LIPs, suggesting a potential involvement of the RAGE transporter on their translocation across the BBB, as proven before for other LIPs with affinity for AB peptides (Markoutsa et al.,

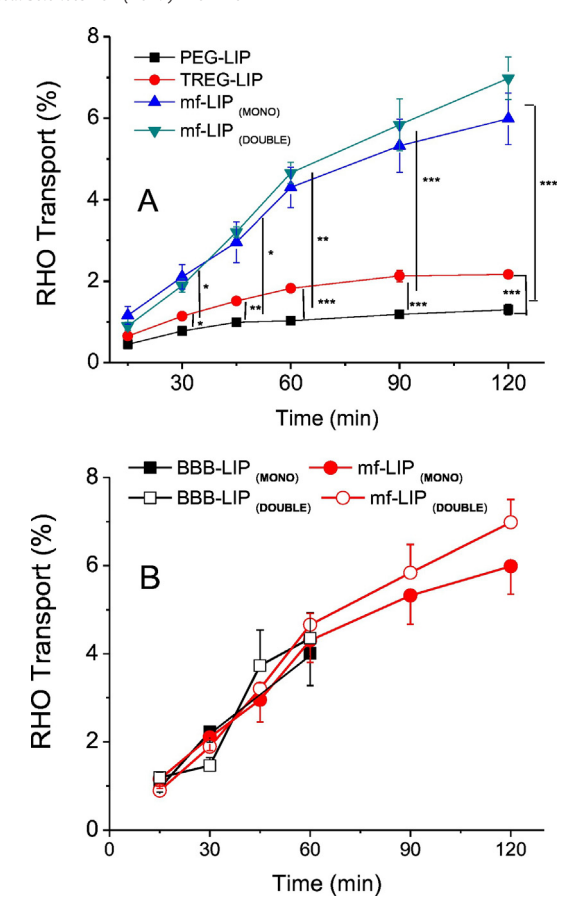


Fig. 5. A] Transport of RHO associated to PEG-LIPs, TREG-LIPs and mf-LIPs (MONO and DOUBLE) across hCMEC/D3 monolayers. B] Comparison of mf-LIPs and BBB-LIPs with MONO density and DOUBLE density, for their transport across hCMEC/D3 monolayers. Each value is the mean of at least 3 experiments. 200 nmoles of lipid from each LIP-type were added per well, and the percent of LIP-associated RHO transported across the monolayer was measured at various time points up to 2 h. Asterisks denote significant differences between specified samples (*P \leq 0.05, **P \leq 0.01, ***P \leq 0.001).

2012). (iii) mf-LIPs and BBB-LIPs seem to have similar capability to be translocated across the BBB, suggesting that the brain-targeting ligands are still functional in the presence of TREG, or that perhaps the ability of TREG to enhance the translocation of vesicles across the BBB (via the RAGE transporter) overrules any potential decrease of BBB-specific ligand functionality, which may be caused by the co-presence of TREG on the vesicle surface (Fig. 5).

The uptake of mf-LIPs by hCMEC/D3 was demonstrated to be slightly lower (by ~15%) compared to that of BBB-LIPs. In order to exploit the later results in light of previous reports about the effect of serum proteins on targeted nanoformulations (Salvati et al., 2013a, 2013b; Markoutsa et al., 2014), the uptake of LIPs by hCMEC/D3 cells was additionally evaluated in the presence of increased concentrations of serum proteins (20–50% v/v). As demonstrated in Fig. 4.B, although the uptake of BBB-LIPs by hCMEC/D3 cells gradually decreases when the experiment is carried out in presence of increasing concentrations of serum proteins (in agreement with previous results), the uptake of mf-LIPs is not affected. In the same context, although ApoE-LIP uptake by hCMEC/D3 cells was highly affected by serum proteins (Markoutsa et al., 2014) which was also confirmed in this study, when TREG is added on ApoE-LIPs, the effect of serum proteins on their cellular uptake is diminished (Fig. 4.C). The two later results suggest a potential role of TREG in lowering the involvement of serum proteins on the interaction between targeted-LIPs and cells. The effect of TREG on reducing potential interactions between LIPs and serum proteins may also be connected with the increased integrity demonstrated for mf-LIPs compared to BBB-LIPs during their incubation in presence of FCS (Fig. 1), although

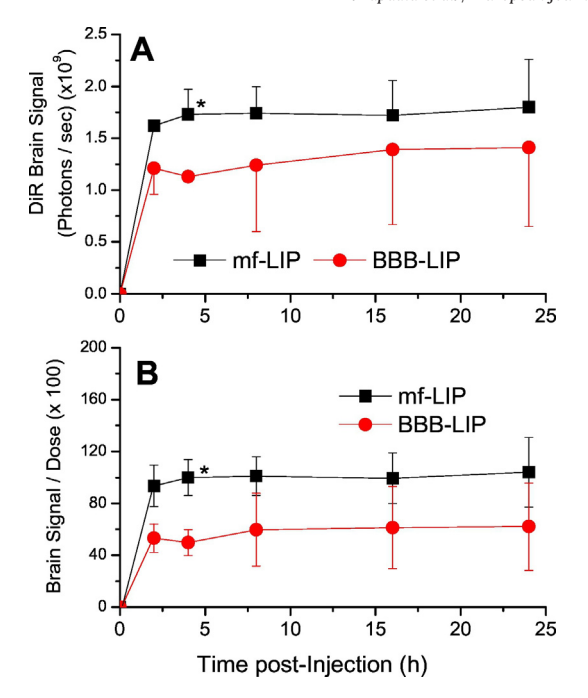


Fig. 6. DiR Brain signals (Photons/s) followed for up to 24 h post-injection by live animal imaging after iv injection of 0.05 mg of liposomal lipid/mouse of mf-LIPs and BBB-LIPs in FVB mice. LIPs with DOUBLE density of the two brain-targeting ligands were tested. Brain Signals are expressed as DiR signals (Photons/s) (A) or Dir signals normalized for the DiR-dose (B). Each value is the mean from 3 to 5 mice and the SD values are denoted by error-bars. Asterisks denote significant differences between mf-LIP and BBB-LIP at specified time points (*P \leq 0.05, **P \leq 0.01, ***P \leq 0.001).

we cannot at this point suggest potential explanations about the specific mechanisms involved. Nevertheless, based on the previously reported theory (Markoutsa et al., 2014), mf-LIPs are expected to have similar in vivo brain targeting capability compared to BBB-LIPs; which is in good agreement with the results of the preliminary live animal imaging in vivo study (Fig. 6); more in vivo studies are currently underway.

Concluding, the capability of multifunctional liposomes (mf-LIPs) to inhibit amyloid peptide aggregation and also efficiently target the BBB, was demonstrated for the first time with liposomes that are functionalized with a curcumin-lipid derivative (as a ligand to increase their affinity towards amyloid species). Despite the complexity of the mf-LIPs tested herein, it was demonstrated that such formulations can be stable under similar conditions to those applying in vivo, and furthermore that the TREG curcumin derivative retains its functionality and at the same time does not reduce the functionality of BBB-specific ligands, when they are all immobilized on the surface of the same vesicle.

The current findings are particularly important due to the lack of widespread BBB disruption in AD, which was recently demonstrated in AD mice-models (Bien-Ly et al., 2015; Zhang et al., 2014). In accordance, any nanotechnology developed as an AD theragnostic system is required to be efficiently translocated across the BBB.

Conflict of Interest

The authors declare that they have no conflict of interest.

Acknowledgements

The research leading to these results has received funding from the European Community's Seventh Framework Programme (FP7/2007–2013) under grant agreements n° 212043 (to SGA) and 260524 (to GTS).

Appendix A. Supplementary Data

Supplementary data to this article can be found online at http://dx.doi.org/10.1016/j.ejps.2017.02.019.

References

Antimisiaris, S.G., 2014. Potential of nanoliposomes for the therapy and/or diagnosis of Alzheimer's disease: recent progress. Clin. Lipidol. 9, 477–481.

Antimisiaris, S.G., Mourtas, S., Markoutsa, E., Skouras, A., Papadia, K., 2014. Nanoparticles for diagnosis and/or treatment of Alzheimer's disease. In: Tiwari, A. (Ed.), Advanced Healthcare Materials. John Wiley & Sons, Inc., Hoboken, NJ, USA http://dx.doi.org/10.1002/9781118774205.ch4.

Aparicio-Blanco, J., Martín-Sabroso, C., Torres-Suárez, A.I., 2016. In vitro screening of nanomedicines through the blood brain barrier: a critical review. Biomaterials 103, 229–255.

Bae, S., Ma, K., Kim, T.H., Lee, E.S., Oh, K.T., Park, E.S., Lee, K.C., Youn, Y.S., 2012. Doxorubicin-loaded human serum albumin nanoparticles surface-modified with TNF-related apoptosis-inducing ligand and transferrin for targeting multiple tumor types. Biomaterials 33. 1536–1546.

Balducci, C., Mancini, S., Minniti, S., La Vitola, P., Zotti, M., Sancini, G., Mauri, M., Cagnotto, A., Colombo, L., Fiordaliso, F., Grigoli, E., Salmona, M., Snellman, A., Haaparanta-Solin, M., Forloni, G., Masserini, M., Re, F., 2014. Multifunctional liposomes reduce brain β-amyloid burden and ameliorate memory impairment in Alzheimer's disease mouse models. J. Neurosci. 34, 14022–14031.

Bana, L., Minniti, S., Salvati, E., Sesana, S., Zambelli, V., Cagnotto, A., Orlando, A., Cazzaniga, E., Zwart, R., Scheper, W., Masserini, M., Re, F., 2014. Liposomes bi-functionalized with phosphaticia caid and an ApoE-derived peptide affect Aβ aggregation features and cross the blood-brain-barrier: implications for therapy of Alzheimer disease. Nanomedicine 10, 1583–1590.

Bien-Ly, N., Boswell, C.A., Jeet, S., Beach, T.G., Hoyte, K., Luk, W., Shihadeh, V., Ulufatu, S., Foreman, O., Lu, Y., DeVoss, J., van der Brug, M., Watts, R.J., 2015. Lack of widespread BBB disruption in Alzheimer's disease models:focus on therapeutic antibodies. Neuron 88. 289–297.

Buchwald, P., Bodor, N., 2016. Brain-targeting chemical delivery systems and their cyclodextrin-based formulations in light of the contributions of Marcus E. Brewster. J. Pharm. Sci. 105, 2589–2600.

Dan, M., Cochran, D.B., Yokel, R.A., Dziubla, T.D., 2013. Binding, transcytosis and biodistribution of anti-PECAM-1 iron oxide nanoparticles for brain-targeted delivery. PLoS ONE 8 (11), e81051.

Fu, S., Xia, J., Wu, J., 2016. Functional chitosan nanoparticles in cancer treatment. J. Biomed. Nanotechnol. 12, 1585–1603.

Gao, H., Qian, J., Cao, S., Yang, Z., Pang, Z., Pan, S., Fan, L., Xi, Z., Jiang, X., Zhang, Q., 2012. Precise glioma targeting of and penetration by aptamer and peptide dual-functioned nanoparticles. Biomaterials 33, 5115–5123.

Gutkin, A., Cohen, Z.R., Peer, D., 2016. Harnessing nanomedicine for therapeutic intervention in glioblastoma. Expert Opin. Drug Deliv. 13, 1573–1582.

Kibria, G., Hatakeyama, H., Ohga, N., Hida, K., Harashima, H., 2011. Dual-ligand modification of PEGylated liposomes shows better selectivity and efficient gene delivery. J. Control. Release 153, 141–148.

Kluza, E., Jacobs, I., Hectors, S.J.C.G., Mayo, K.H., Griffoen, A.W., Strijkers, G.J., Nicolay, K., 2012. Dual-targeting of ανβ3 and galectin-1 improves the specificity of paramagnetic/fluorescent liposomes to tumor endothelium in vivo. J. Control. Release 158, 207–214

Koffie, R.M., Farrar, C.T., Saidi, L.-J., William, C.M., Hyman, B.T., Spires-Jones, T.L., 2011. Nanoparticles enhance brain delivery of blood-brain-barrier-impermeable probes for in vivo optical and magnetic resonance imaging. PNAS 108, 18837–18842.

Kokona, M., Kallinteri, P., Fatouros, D., Antimisiaris, S.G., 2000. Stability of SUV liposomes in the presence of cholate salts and pancreatic lipases: effect of lipid composition. Eur. J. Pharm. Sci. 9, 245–252.

Lalani, J., Raichandani, Y., Mathur, R., Lalan, M., Chutani, K., Mishra, A.K., Misra, A., 2012. Comparative receptor based brain delivery of tramadol-loaded poly(lactic-co-glycolic acid) nanoparticles. J. Biomed. Nanotechnol. 8, 918–927.

Lazar, A., Mourtas, S., Youssef, I., Parizot, C., Dauphin, A., Delatour, B., Antimisiaris, S.G., Duyckaerts, C., 2013. Curcumin-conjugated nanoliposomes with high affinity for Aβ deposits: possible applications to Alzheimer disease. Nanomed.: Nanotechnol., Biol. Med. 9, 712–721.

Li, Y., He, H., Jia, X., Lu, W.-L., Lou, J., Wei, Y., 2012. A dual-targeting nanocarrier based on poly(amidoamine) dendrimers conjugated with transferrin and tamoxifen for treating brain gliomas. Biomaterials 33, 3899–3908.

Ma, J., Porter, A.L., Aminabhavi, T.M., Zhu, D., 2015. Nano-enabled drug delivery systems for brain cancer and Alzheimer's disease: research patterns and opportunities. Nanomedicine 11, 1763–1771.

Manzoni, C., Colombo, L., Messa, M., et al., 2009. Overcoming synthetic Abeta peptide aging: a new approach to an age-old problem. Amyloid 16, 71–80.

Markoutsa, E., Pampalakis, G., Niarakis, A., Romero, I.A., Weksler, B., Couraud, P.-O., Antimisiaris, S.G., 2011. Uptake and permeability studies of BBB-targeting immunoliposomes using the hCMEC/D3 cell line. Eur. J. Pharm. Biopharm. 77, 265–274

Markoutsa, E., Papadia, K., Clemente, C., Flores, O., Antimisiaris, S.G., 2012. Anti-Aβ-MAb and dually decorated nanoliposomes: effect of Aβ1-42 peptides on interaction with hCMEC/D3 cells. Eur. J. Pharm. Biopharm. 81, 49–56.

Markoutsa, E., Papadia, K., Giannou, A.T., Spella, M., Cagnotto, A., Salmona, M., Stathopoulos, G.T., Antimisiaris, S.G., 2014. Mono and dually decorated

- nanoliposomes for brain targeting, in vitro and in vivo studies. Pharm. Res. 31, 1275–1289.
- Markoutsa, E., Mourtas, S., Bereczki, E., Zona, C., La Ferla, B., Nicotra, F., Flores, O., Pei, J.-J., Antimisiaris, S.G., 2015. Comparison of various types of ligand decorated nanoliposomes for their ability to inhibit amyloid aggregation and to reverse amyloid cytotoxicity. Curr. Top. Med. Chem. 15. 2267–2276.
- Mourtas, S., Canovi, M., Zona, C., Aurilia, D., Niarakis, A., La Ferla, B., Salmona, M., Nicotra, F., Gobbi, M., Antimisiaris, S.G., 2011. Curcumin-decorated nanoliposomes with very high affinity for amyloid-b1-42 peptide. Biomaterials 32, 1635–1645.
- Mourtas, S., Lazar, A.N., Markoutsa, E., Duyckaerts, C., Antimisiaris, S.G., 2014. Multifunctional nanoliposomes with curcumin-lipid derivative and brain targeting functionality with potential applications for Alzheimer disease. Eur. J. Med. Chem. 80, 175–183.
- Nair, M., Jayant, R.D., Kaushik, A., Sagar, V., 2016. Getting into the brain: potential of nanotechnology in the management of NeuroAIDS. Adv. Drug Deliv. Rev. 103, 202–217.
- Papadia, K., Markoutsa, E., Antimisiaris, S.G., 2016. How do the physicochemical properties of nanoliposomes affect their interactions with the hCMEC/D3 cellular model of the BBB? Int. I. Pharm. 509. 431–438.
- Pardridge, W.M., 2016. CSF, blood-brain barrier, and brain drug delivery. Expert Opin. Drug Deliv. 13, 963–975.
- Poller, R., Gutman, H., Krahenbuhl, S., Weksler, B., Romero, I., Couraud, P.O., Tuffin, G., Drewe, J., Huwyler, J., 2008. The human brain endothelial cell line hCMEC/D3 as a human blood-brain barrier model for drug transport studies. J. Neurochem. 107, 1358–1368
- Re, F., Cambianica, I., Zona, C., Sesana, S., Gregori, M., Rigolio, R., La Ferla, B., Nicotra, F., Forloni, G., Cagnotto, A., Salmona, M., Masserini, M., Sancini, G., 2011. Functionalization of liposomes with ApoE-derived peptides at different density affects cellular uptake and drug transport across a blood-brain barrier model. Nanomed.: Nanotechnol., Biol. Med. 7, 551–559.
- Rotman, M., Welling, M.M., Bunschoten, A., de Backer, M.E., Rip, J., Nabuurs, R.J.A., Gaillard, P.J., van Buchem, M.A., van der Maarel, S.M., Van der Weerd, L., 2015. Enhanced glutathione PEGylated liposomal brain delivery of an anti-amyloid single domain anti-body fragment in a mouse model for Alzheimer's disease. J. Control. Release 203, 40–50.

- Salvati, A., Pitek, A.S., Monopoli, M.P., Prapainop, K., Baldelli-Bombelli, F., Hristov, D.R., Kelly, P.M., Åberg, C., Mahon, E., Dawson, K.A., 2013a. Transferrin-functionalized nanoparticles lose their targeting capabilities when a biomolecule corona adsorbs on the surface. Nat. Nanotechnol. 8, 137–143.
- Salvati, E., Re, F., Sesana, S., Cambianica, I., Sancini, G., Masserini, M., Gregory, M., 2013b. Liposomes functionalized to overcome the blood-brain barrier and to target amyloid-beta peptide: the chemical design affects the permeability across an in vitro model. Int. J. Nanomedicine 8, 1749–1758.
- Saraiva, C., Praça, C., Ferreira, R., Santos, T., Ferreira, L., Bernardino, L., 2016. Nanoparticle-mediated brain drug delivery: overcoming blood-brain barrier to treat neurodegenerative diseases. J. Control. Release 235, 34–47.
- Stewart, J.C.M., 1980. Colorimetric determination of phospholipids with ammonium ferrothiocyanate. Anal. Biochem. 104, 10–14.
- Tam, V.H., Sosa, C., Liu, R., Yao, N., Priestley, R.D., 2016. Nanomedicine as a non-invasive strategy for drug delivery across the blood brain barrier. Int. J. Pharm. 515, 331–342.
- Taylor, M., Moore, S., Mourtas, S., Niarakis, A., Re, F., Zona, C., La Ferla, B., Nicotra, F., Masserini, M., Gregori, M., Antimisiaris, S.G., Allsop, D., 2011. Effect of curcumin-associated and lipid ligand functionalised nanoliposomes on aggregation of the Alzheimer's Aβ peptide. Nanomed.: Nanotechnol., Biol. Med. 7, 541–550.
- Wong, H.L., Wu, X.Y., Bendayan, R., 2012. Nanotechnological advances for the delivery of CNS therapeutics. Adv. Drug Deliv. Rev. 64, 686–700.
- Ye, D., Nic Raghnaill, M., Bramini, M., Mahon, E., Åberg, C., Salvati, A., Dawson, K.A., 2013. Nanoparticle accumulation and transcytosis in brain endothelial cell layers. Nanoscale 5, 11153–11165.
- Zhang, C., Wan, X., Zheng, X., Shao, X., Liu, Q., Zhang, Q., Qian, Y., 2014. Dual-functional nanoparticles targeting amyloid plaques in the brains of Alzheimer's disease mice. Biomaterials 35, 456–465.
- Zhang, D., Wang, J., Xu, D., 2016. Cell-penetrating peptides as noninvasive transmembrane vectors for the development of novel multifunctional drug-delivery systems. J. Control. Release 229, 130–139.